Spectral Simulation of Heat Transfer Across Polytype Interfaces

Nadjib Izitounene, Ngoc Duc Le, Brice Davier, Philippe Dollfus, Lorenzo Paulatto, Jérome Saint-Martin

WILEY-VCH

Spectral simulation of heat transfer across polytype interfaces

*Nadjib Izitounene, Ngoc Duc Le, Brice Davier, Philippe Dollfus, Lorenzo Paulatto and Jérome Saint-Martin**

N. Izitounene, N. D. Le, P. Dollfus, J. Saint-Martin

Université Paris-Saclay, CNRS, Centre de Nanosciences et de Nanotechnologies, 91120, Palaiseau, France

E-mail: jerome.saint-martin@u-psud.fr

L. Paulatto

Sorbonne Université/CNRS/MNHN/IRD UMR 7590, Institut de Minéralogie, de Physique des Matériaux et de Cosmochimie

Keywords: Polytype, Nanowire, Monte Carlo, Thermal, Simulation

Polytype nanowires fabricated in both silicon and germanium are particularly attractive for thermoelectric engineering. In this work, the transport of phonons across polytype heterojunction such as Si 3C/Si 2H and Ge 3C/Ge 2H is theoretically studied by using a particle Monte Carlo simulation for phonons. Full-Band dispersions and phonon-phonon scattering rates are calculated by using the density-functional theory (DFT). Phonon transmission across interfaces are implemented by using a Full-Band version of the Diffusive Mismatch Model (DMM).

First, the different transport regimes (diffusive, ballistic and intermediate) for homogenous 3C and 2H Si and Ge bars are investigated by using the Knudsen number as well as the spectral contributions of the thermal flux.

Then, single and double polytype Si and Ge heterostructures are studied. The variation of the interface thermal conductance as a function of the geometric dimension as well as the effects of the spectral distribution of the flux are investigated. This local indicator of the phonon transport regime can be used as a local indicator of the occurrence the out of equilibrium transport regime. Finally, it is shown that the polytype interfaces exhibit significant thermal resistances and generate an out of equilibrium phonon transport regime around the interface over several nanometers.

1. Introduction

To harvest the large amount of thermal losses released into the environment [1], the use of thermoelectric (TE) generators that directly convert heat into electricity is appealing to power small electronic systems [2]. This conversion requires material having both good electrical conductivity and poor thermal conductivity, leading to the concept of "Phonon-Glass Electron-Crystals". These properties are rare in nature and the main commercial TE module exhibiting the best (but modest) thermoelectric efficiency are made of a BiTe alloy using atomic species that are toxic and not abundant on earth.

However, since the theoretical prediction of Hicks and Dresselhaus [3], nanostructuring has been used to boost the thermoelectric performance [4]. In particular, thermoelectric nanostructures are designed to benefits from the fact that at the nanoscale the mean free path (mfp) of phonons is usually significantly higher than that of electrons [4]. For instance, the presence of interfaces separated by a distance in the order of magnitude of the phonon mfp is expected to significantly degrade the thermal properties while degrading marginally the electron transport. In addition, nonlinear transport properties around interfaces could be used to improve the Seebeck coefficient [5], [6]. In this context, a polytype interface, i.e. an interface separating two phases of the same material, seems of high potential. This kind of interface involving both the of cubic 3C and hexagonal 2H phases can be processed in nanowires made of Silicon [7] or Germanium [8] that may even exhibit a high density of polytype interface (which remains currently difficult to control in terms of position and quality). Since based on the most standard materials of the semi-conductor industry, such nanostructures are thus particularly attractive to boost thermoelectric efficiency.

To theoretically investigate these nanostructures, the Fourier heat equation is poorly relevant. Indeed, at the nanoscale the phonon transport regime is barely diffusive but often out of equilibrium, i.e. fully or quasi ballistic. To characterize the transport regime, the Knudsen number, defined as the ratio of the mfp to the system length, is commonly considered [9]. However, this parameter is an average material parameter that cannot be used as a local indicator of the transport regime inside a nanodevice.

Moreover, the modeling of the interface by an interfacial thermal resistance (or Kapitza's resistance [10]) requires an accurate description of the phonon flux across the interface and above all a relevant definition of the temperature on each side of the interface [11] [12]. The introduction of hemispherical temperature, naturally available from particle Monte Carlo simulation, is required to estimate accurately the interface thermal conductance [13]. Besides, the simulation of phonon transport across polytype interface in which there is no atomic mass mismatche requires an atomistic approach or at least a full band description of the phonon dispersion on each side of the interface.

Among the available numerical modeling techniques for the heat transport at the nanoscale, including that based on the Non-equilibrium Green Function approach (NEGF) [14], [15], the Molecular Dynamics (MD) [16]–[18], or the hydrodynamic equation, the particle Monte Carlo method [19]–[21] is interesting as it naturally captures all transport regimes with all details on the spectral properties of phonon transport. This transport formalism which solves stochastically the Boltzmann transport equation is able to consider at equilibrium the Bose-Einstein statistics and can thus be used in a wide temperature range including the temperature below the Debye's temperature.

In this work, a homemade Full Band Monte Carlo simulator [22] [23] dedicated to the phonon transport has been used to investigate the thermal transport across simple and multiple 3C/2H polytype interfaces of Silicon and Germanium. The material properties such as the phonon dispersion and relaxation rates in the 3D Brillouin zone (BZ) were computed using ab-initio

computation [24]. The phonon transmission across interfaces was implemented in the Full Band Monte Carlo simulator for phonons [22], [23] by using a Full-band version of the Diffusive Mismatch Model (DMM) [25], [26].

The present work focuses on the spectral and modal properties of transport to locally characterize the out of equilibrium phonon transport regime occurring around the interfaces. In section 2, the MC simulator and the simulated devices are presented. In section 3, the phonon flux crossing the interfaces is investigated and the related thermal interface conductances are discussed. The spectral and modal contributions are analyzed in the last section.

2. Full Band Monte Carlo Model

2.1. Ab-initio material description

Two materials have been investigated, i.e. Si and Ge, in both their hexagonal (2H) and cubic (3C) forms. The latter one being quite well known, we emphasized our study on the hexagonal phase and, especially, on the 2H/3C interfaces of these materials. It should be noted that we have studied here the bulk properties of the 2H and 3C phases, because even for nanowires, these properties remain relevant for systems larger than a few tens of nanometers [27].

Full Band Monte Carlo simulations require the prior knowledge of phonon dispersions, phonon group velocities and phonon scattering rates.

Ab-initio calculations were performed using the Quantum ESPRESSO [28] code, the energy functional is approximated with the LDA-PZ [29] local density approximation which gives good agreement for the lattice geometry for pure Silicon and Germanium. The ions were modeled using norm-conserving pseudopotentials adapted from the SG15 ONCV library [30], keeping the same pseudization radii. The charge density has been expanded up to a kinetic energy cutoff of 50 Ry and integrated over a regular shifted grid of 8×8×8 electronic kpoints for cubic structures, and 8×8×4 k-points for the 2H structures. Harmonic 2-body force constants are obtained by Fourier transform of a density-functional perturbation theory [31] over a 8×8×8 (cubic) or 8×8×4 (2H) grid of q-points, while anharmonic 3-body force constant are computed ab-initio over a shorter range grid of 4×4×4 (cubic) or 4×4×2 (2H) q-points. From these force constants, the 2nd and 3rd order dynamical matrices can be obtained at any q-points via Fourier interpolation [32]. This interpolation is carried on over a grid of 29×29×29 (29×29×21) q-points for the cubic (2H) structure, in order to integrate the intrinsic lifetime of any phonon. The integration calculation is repeated for every point in an "outer" grid of 31×31×31 (19×19×13) q-points to sample the lifetime of the entire BZ. The properties of Fourier transform can also be used to interpolate the phonon group velocity at any q-points.

The DFT calculation allowed us to determine the forces acting on the atoms, from which the harmonic and anharmonic force constants have been extracted. The phonon frequency and group velocity can then be computed from the dynamical matrix, together with the scattering rates corresponding to phonon–phonon interactions. In the conventional 3C phase, there are six phonon modes, i.e. two transverse acoustic (TA), one longitudinal acoustic (LA), one longitudinal optical (LO) and two transverse optical (TO) modes, in the case of the 2H phase with four atoms per unit cell, there are up to twelve modes, including nine optical modes.

The phonon dispersion for both Ge 2H and Si 2H materials is shown in Figure 1 in the form of iso-energy cartography of the first phonon mode in some specific planes, which illustrates the strong anisotropy of the lattice vibrations modes, except at very low frequency where the iso-frequency contour are not far from being circular.

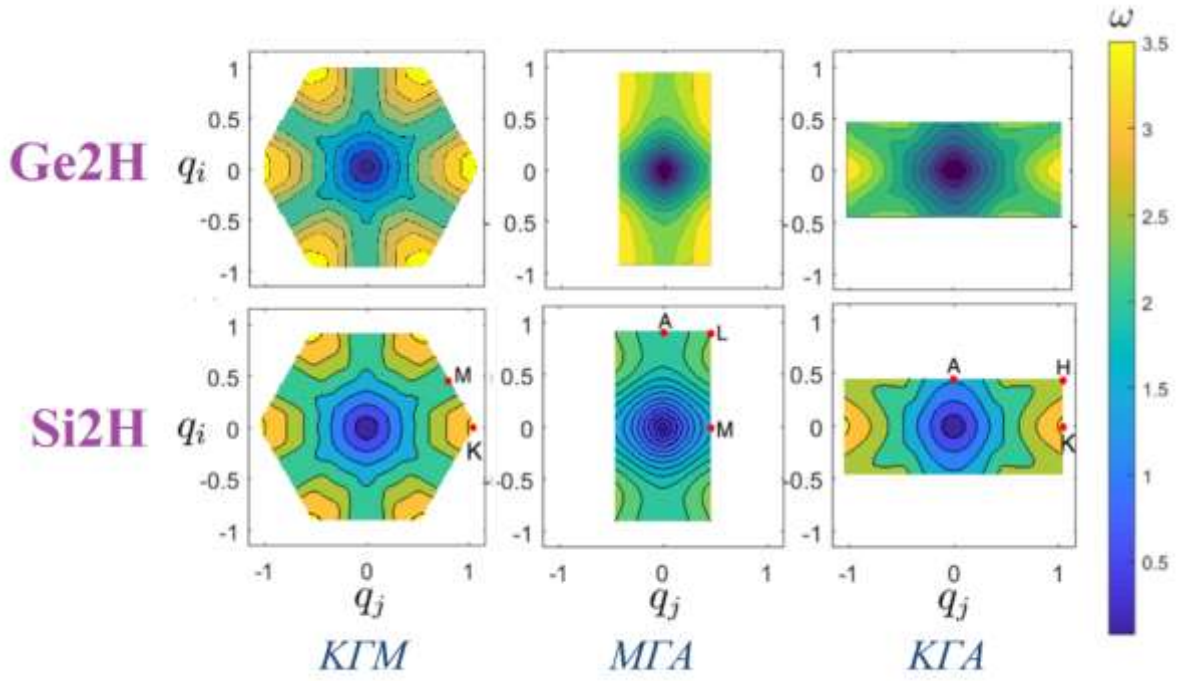

Figure 1. Cartography of the angular frequency ω in the BZ of (top) Ge 2H and (bottom) Si 2H. Angular frequencies are given in [10^{13} 2π/s]. In left, middle and right panels, the iso-frequencies contours are plotted in the (10-10), (11-20) and (0001) planes, respectively.

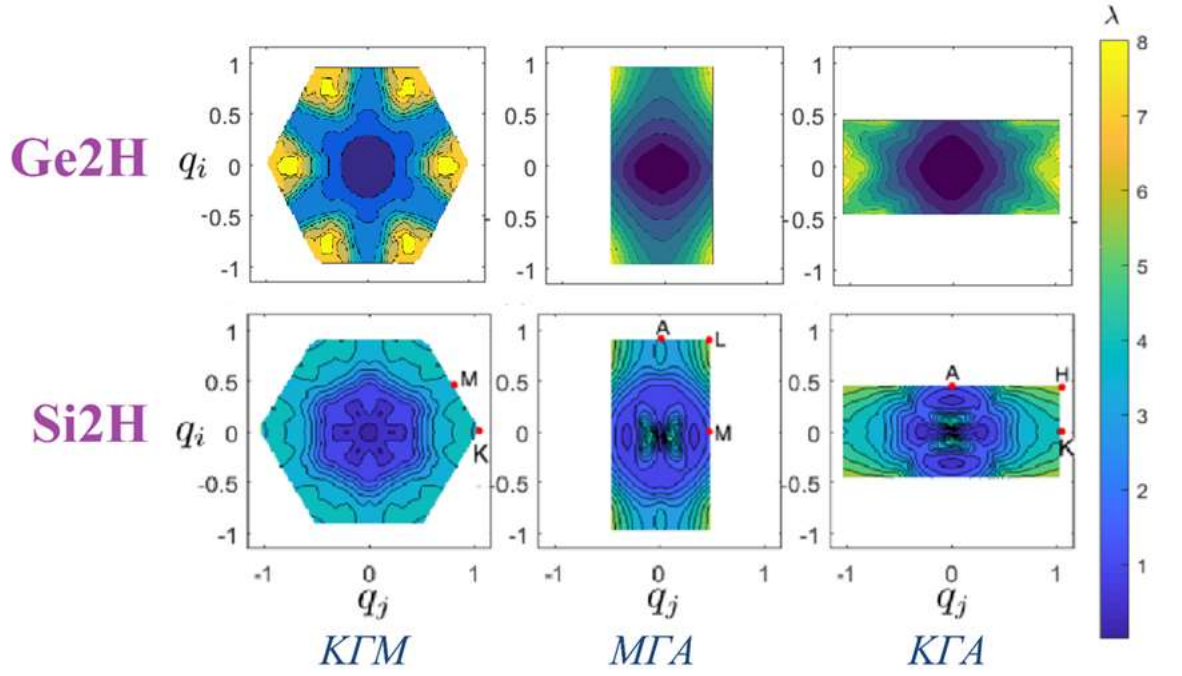

Figure 2. Cartography of phonon-phonon scattering rates λ in the BZ for the first phonon mode. Scattering rates are given in [10^{10} Hz]. In left, middle and right panels, the iso-rates are plotted for the (10-10), (11-20) and (0001) planes, respectively.

Figure 2 shows the cartography of scattering rates for both hexagonal materials at 300 K. Scattering rates were calculated for 101 values of temperature ranging from 0 K to 1000 K, though the present study focuses on temperatures around 300 K.

The anisotropy of both scattering rates and the phonon dispersion is important which justifies the requirement of implementing a Full-Band phonon description within the Monte Carlo transport model.

2.2. Particle Monte Carlo method for phonon transport

The particle Monte Carlo method used here consists in solving the time-dependent Boltzmann equation for phonons by describing the stochastic behaviour of large number of phonons considered as classical particles, without any assumption on the shape of the phonon distribution function. The trajectories of particles, i.e. the times of free-flight and the type and effect of scattering event experienced after each free-flight, are randomly selected according to all relevant scattering rates. Here, the previously described full-band phonon dispersion and scattering rates are used as material input parameters for the MC simulation.

The phonon-phonon scattering mechanisms are implemented by using the two-phonon approach developed in [20]. To ensure energy conservation, each simulated particle (which corresponds to a phonon packet) carries the same energy. This means that for different phonon modes (i.e. for different wave vectors or polarizations), a simulated particle represents a different number of (real) phonons, but all simulated particles carry the same energy. Besides a variance reduction method [33] is used to reduce the simulation time. This approach tends to limit the number of simulated phonons to those that are actually involved in heat transport, i.e. those that differs from the Bose-Einstein statistics.

The values of the local pseudo-temperature at each position in the structure are updated according to the local (and exact) phonon distributions at each time step.

The contacts with the external thermostats are assumed to be perfect emitters and absorbers.

All the details of the Monte Carlo algorithm employed in this work may be found in Ref.[20].

2.3. Thermal parameters

As detailed in Ref. [13], the hemispherical temperatures T^+ and T^- are defined, even in out-of-equilibrium conditions, as the temperature of phonon sub-populations with a positive/negative (oriented toward the cold/hot thermostat, respectively) giving the same energy density E as that obtained from an equilibrium distribution. Thus, it satisfies the following relationship:

$$E(T^{\pm}) = \frac{\Omega}{(2\pi)^3} \sum_{state\ s,\ v_x^s > \frac{0}{v_x^s} < 0} \hbar\omega_s f_{BE}(\omega_s, T^{\pm}) \quad (1)$$

Where Ω is the volume of the considered reciprocal space f_{BE} is the Bose-Einstein distribution function and ω_s the phonon angular frequency of state s.

These temperatures are instrumental to work out a realistic value of the interface conductance G_{int} in heterostructures [13]:

$$G_{int} = \frac{Q}{\Delta T^I} = \frac{Q}{T^+(x-\varepsilon) - T^-(x+\varepsilon)} \quad (2)$$

where the local temperature difference at interface $\Delta T^I = T^+(x-\varepsilon) - T^-(x+\varepsilon)$ is the difference between the hemispherical temperatures on each side of the interface.

In a 1D homogeneous system of length L in contact with a hot thermostat at a hot temperature T_H and a cold one at a cold temperature T_C, the thermal flux Q can be expressed (in all transport regimes) by using these different formulae:

$$Q = G_{total}.\Delta T_{contact} = \kappa_{eff} \frac{\Delta T_{contact}}{L} = \kappa_{ballistic} \frac{\Delta T_{local}}{L} \quad (3)$$

where the two temperature differences are defined as follows:

$$\Delta T_{local}(x) = T^{+}(x) - T^{-}(x)$$

$$\Delta T_{contact} = T_H - T_C.$$

For a homogeneous structure in which a temperature bias $\Delta T_{contact}$ is applied and working at (pseudo) temperature $\bar{T}$, the thermal conductivity $\kappa_{effective}$ is given by (cf. [34]):

$$\kappa_{effective} = \frac{Q}{\Delta T_{contact}} = \frac{\Omega}{(2\pi)^3} \sum_{state\ s} \hbar\omega_s \left| v_{s,x} \right| \lambda_{eff,s} . \frac{\partial f_{BE}}{\partial T}(\omega_s, \bar{T}) \quad (4)$$

where Ω is the volume of the first Brillouin zone, $\lambda_{eff,s} = \frac{\lambda_{mfp,s}}{1 + L/(2.\lambda_{mfp,s})}$ in which $\lambda_{mfp,s}$ the mean free path of phonon mode *s* and $v_{s,x}$ is the phonon group velocity of the state *s* along the *x*-direction that is the heat transport direction. In a ballistic system $\lambda_{mfp,s} = L/2$ and thus the ballistic conductivity $\kappa_{ballistic}$ is given by:

$$\kappa_{ballistic} = \frac{L}{2} \frac{\Omega}{(2\pi)^3} \sum_{state\ s} \hbar\omega_s \left| v_{s,x} \right| \frac{\partial f_{BE}}{\partial T}(\omega_s, \bar{T}) \quad (5)$$

Further details on the inner workings of the simulator were given in previous works [13].

2.4. Simulated devices

In this work, homogeneous and heterogeneous nanostructures of length L along the X axis were investigated. In all structures, the thermal flux flows along the X axis, i.e. perpendicular to the thermal contact surfaces located at both ends, with a hot thermostat of temperature $T_H = 302K$ and a cold thermostat of temperature $T_C = 298\ K$, respectively, resulting in a mean temperature of 300 K. Unless otherwise stated, these are the standard temperature settings for the simulations presented here.

In the YZ plane the nanostructures are assumed to have an infinitely large cross-section. To be consistent with this configuration though using a finite rectangular meshing ($\Delta Y = \Delta Z = 100$ nm), periodic boundary conditions were applied to any particle reaching an external surface. First, all structures are uniformly meshed along the X-axis into 20 equally sized cells. Then, the meshing is refined in the vicinity of the interfaces (in the case of heterostructure) and the thermostats. The length of these refined cells located 5 nm around the interfaces are less or equal to 1 nm. This is instrumental in computing a coherent G_{int} value [23].

Figure 3 illustrates the types of devices investigated here:

- Homogeneous devices (a) of length L.
- Simple heterojunctions (b) in which a Diffusive Mismatch Model (DMM) heterojunction (in yellow) is placed at the centre of the structure ($x = L/2$) joining two homogeneous bars.
- Double heterojunctions (not shown in Fig. 3) in which three equally-long homogeneous bars are joined to form two DMM interfaces at positions $x = L/3$ and $x = 2L/3$.

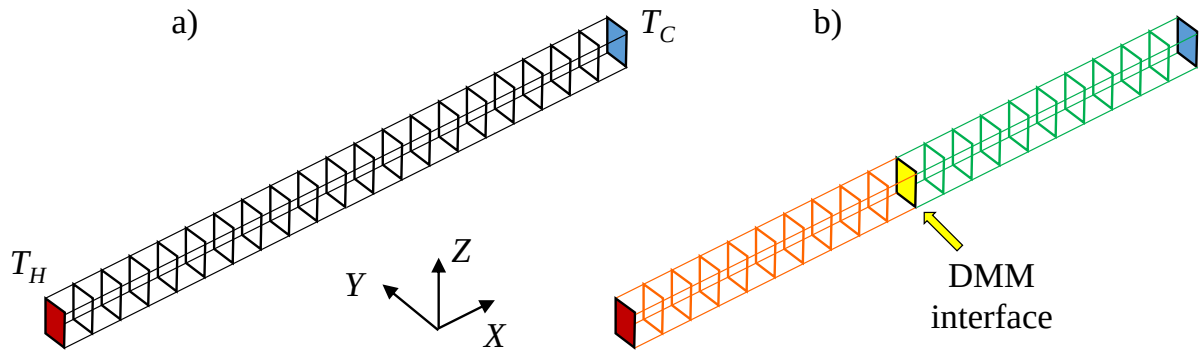

Figure 3. Schema of studied a) homogeneous device and b) heterostructure. Red and blue faces are hot and cold thermostats, respectively. Transparent external faces symbolise that periodic boundary conditions are applied in Y and Z directions.

3. Results and discussion

3.1. Phonon transport regime in homogeneous structures

In previous works, the coherence and effectiveness of the MC method have been proven for Si 3C [22], [23]. Figure 4(a) shows the length dependence of the Knudsen number K_D for homogeneous structures made of Si and Ge, in both 3C and 2H forms. To characterize the different heat transport regimes K_D is computed by using the ratio $\kappa_{effective}/\kappa_{ballistic}$ which is equivalent to the ratio of the mfp to the system length according to Eq. 4 and 5.

Indeed, for lengths smaller than 10 nm, K_D is greater than 0.8, which is typical of a ballistic transport regime. Lengths over 1 µm lead to quasi-diffusive conductivity characterized by $K_D < 0.1$. In between, an intermediary transport regime takes place. The Knudsen number does tend to extremely small values. It can be explained by Figure 4(b), where the conductivity values of different materials grow about 2 orders of magnitude higher than the ballistic conductivity value.

In long devices, the thermal conductivity $\kappa_{effective}$ tends to an asymptotic value, the standard thermal conductivity $\kappa_{diffusive}$ (given by Eq. 4 for $L \rightarrow \infty$) which is 136 $W.m^{-1}.K^{-1}$ (resp. 58 $W.m^{-1}.K^{-1}$) for Si 3C (resp. Ge 3C) at 300 K. These values are in very good agreement with those found in the literature [35].

For a given material, the conductivity values of both 3C and 2H forms are almost identical, which may lead one to believe that cubic and hexagonal phases behave in a very same fashion in all aspects of thermal transport. However, we will see in the final sub-sections that it is not the case.

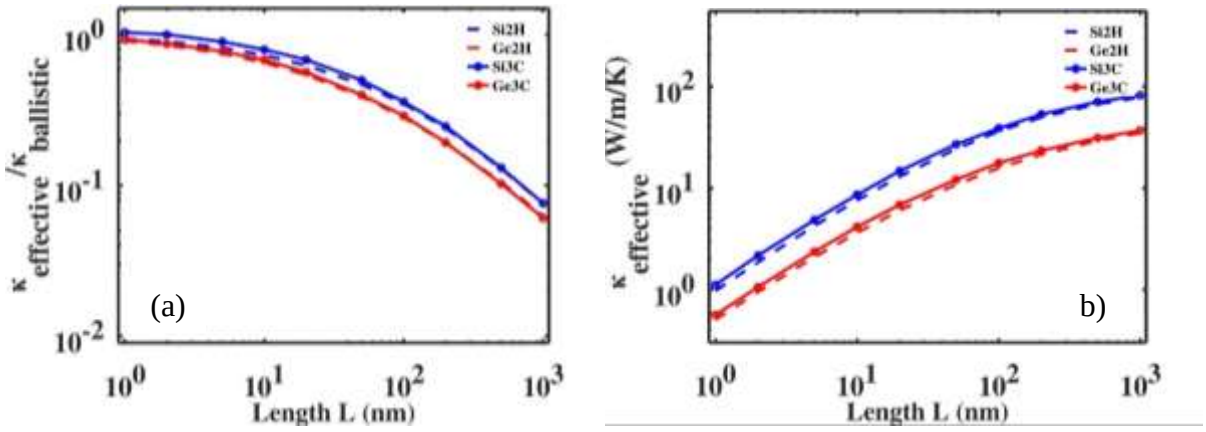

Figure 4. (a) Knudsen number K_D and (b) Thermal conductivity $\kappa_{effective}$ as a function of device length for homogeneous structures at room temperature.

3.2. Interface thermal conductance

In a previous work, different kinds of Si/Ge heterostructures have been studied [23]. Here, different Polytype Si (Si 3C-2H) and Ge (Ge 3C-2H) heterostructure devices have been studied, with total device length ranging from 1 nm to 1000 nm and thermostat temperatures T_H and T_C fixed as previously. We plot in Figure 5 the heat flux density and the interface conductance as

a function of device length. Beyond the fact that both Si and Ge structures behave similarly, the notable tendency here is that a convergence is reached for the interface conductance G_{int}, with $G_{int} \approx 285$ MW.K^{-1}.m^{-2} for Polytype Ge devices and $G_{int} \approx 500$ MW.K^{-1}.m^{-2} for Polytype Si devices. For comparison, these values are very close to those obtained for Si-Ge heterostructures $G_{int} = 220$ MW.K^{-1}.m^{-2} [23], [25]. It may be marginally noted that the MC error bars in the polytype interfaces are significantly smaller in the polytype interface than in the Si/Ge interface although they are calculated with the same methodology [23] (as the calculated heat flux without temperature difference, i.e. the flux resolution, is smaller cf. Figs. 6(a)).

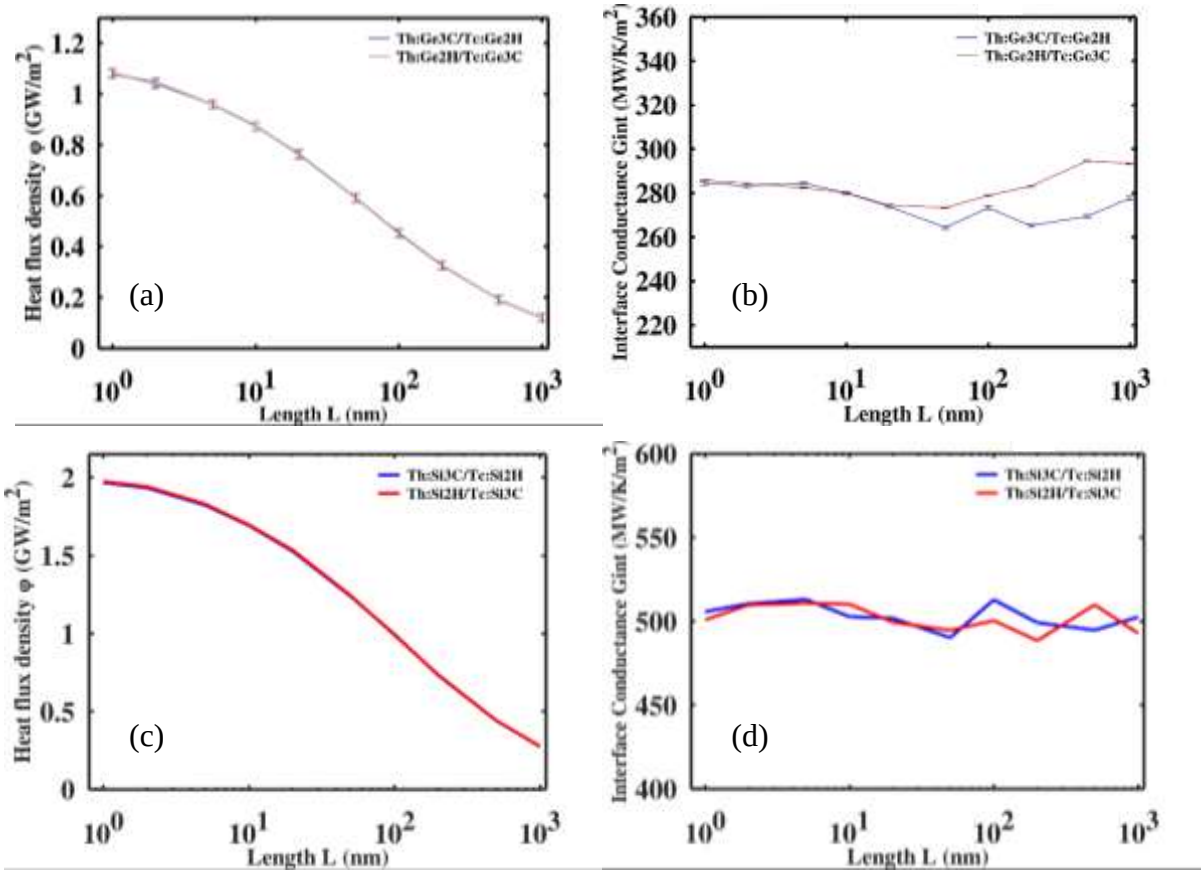

Figure 5. (a,c) Heat flux density and (b,d) Interface conductance for (a,b) Polytype Ge, (c,d) Polytype Si as a function of device length at room temperature.

These values remain the same when considering the influence of the temperature bias of thermostats for a given length. It is shown on Figure 6 for Ge structures. The heat flux density (Fig. 6(a)) and interface thermal conductance (Fig. 6(b)) are plotted as a function of the temperature bias $(T_H\text{-}T_C)$ for 20 nm-long devices. The average value of G_{int} remains very close to that found when studying the influence of length at given temperature bias (see Fig. 5(b)).

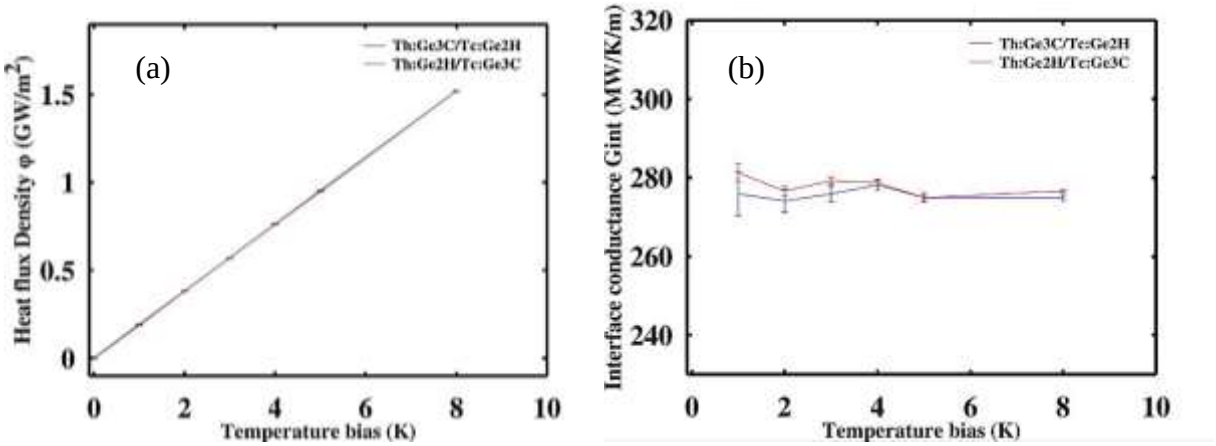

Figure 6. (a) Heat flux density and (b) Interface conductance (B) for Polytype Ge heterostructures as a function of the temperature bias for a given length L = 20 nm.

The fluctuations that are observed in the G_{int} values (Figs. 5(b), 5(d) and 6(b) are inherent in particle MC simulation and tend to increase when increasing the device length. Such fluctuations are less notable in Figure 6 where the length is quite short and fixed to 20 nm, having temperature bias as the only variable. However, the resulting average values are well within error bars, which gives confidence in assigning a value to G_{int} for each type of interface.

3.3. Spectral analysis

Up to now, the heat flux density has been considered as a macroscopic parameter and analyzed as a function of either device length or temperature bias. Figure 7 brings out another manner of viewing the heat flux density: the spectral analysis.

Considering a $T_H = 302K$ and $T_C = 298\ K$, two Polytype Ge (T_H:Ge 3C / T_C:Ge 2H) devices have been studied for two different lengths, i.e. L = 500 nm (Fig. 7(a)) and L = 10 nm (Fig. 7(b)). Spectral heat flux density was extracted at four different positions of the devices. The flux remains untroubled throughout the whole device, whether it be at the middle of the Ge 3C / 2H halves or near the DMM interface of the two phases. A Noisy may be observed for the longer devices (Fig. 7(a)). Nevertheless, the concordance between spectral heat flux before and after the junction is intact. This noisy aspect is still being investigated.

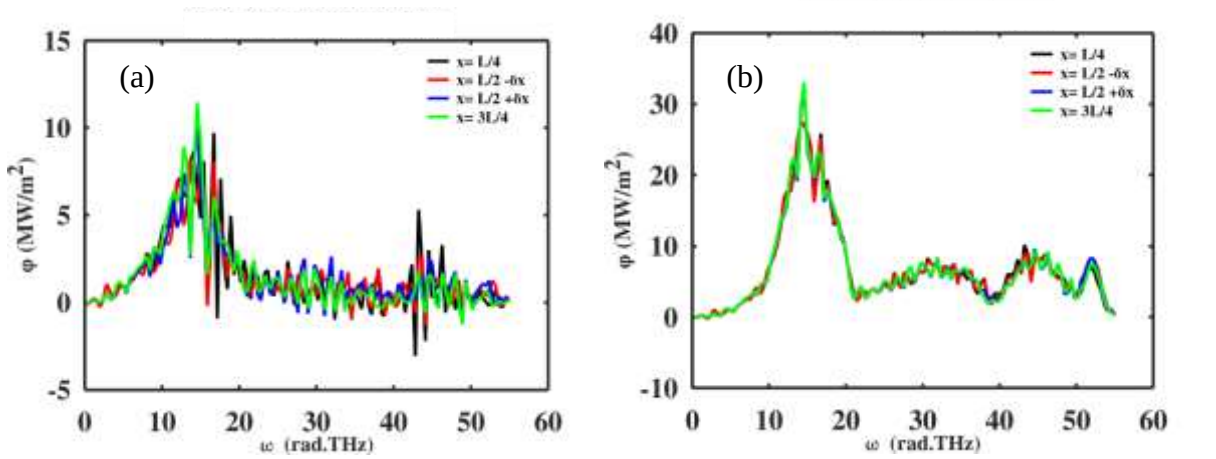

Figure 7 . Spectral heat flux density distribution in Polytype Ge devices at room temperature for (a) L = 500 nm and (b) L = 10 nm.

Figure 7 suggests a strong similarity in the behaviour of phonons in both 3C and 2H Ge phases, consistently with the results of thermal conductivity shown in Fig. 4. Indeed, the two materials

are *basically* the same (phonon density of states are similar in both cases). The flux does not seem to be disturbed by the presence of the phase interface.

This question is investigated in more details in the following sub-section, dedicated to modal contributions of phonons throughout these devices.

3.4. Modal analysis

Figure 8 displays the contributions (in %) of the different phonon modes to the heat transport in a 200 nm-long Polytype Ge device (T_H:Ge 3C / T_C:Ge 2H) with standard temperature conditions ($T_H = 302\ K$ and $T_C = 298\ K$).

Along the device, the six phonon modes of cubic Ge (left side) turn into the twelve modes of hexagonal Ge (right side). The total heat flux transmission through the interface is conserved, as shown in the previous section. However, the modes are significantly disturbed when passing through the interface, except for the Longitudinal Optical one. In order to conserve the flux and allow all modes to contribute, the contributions of the acoustic branches are lower in the 2H half of the device.

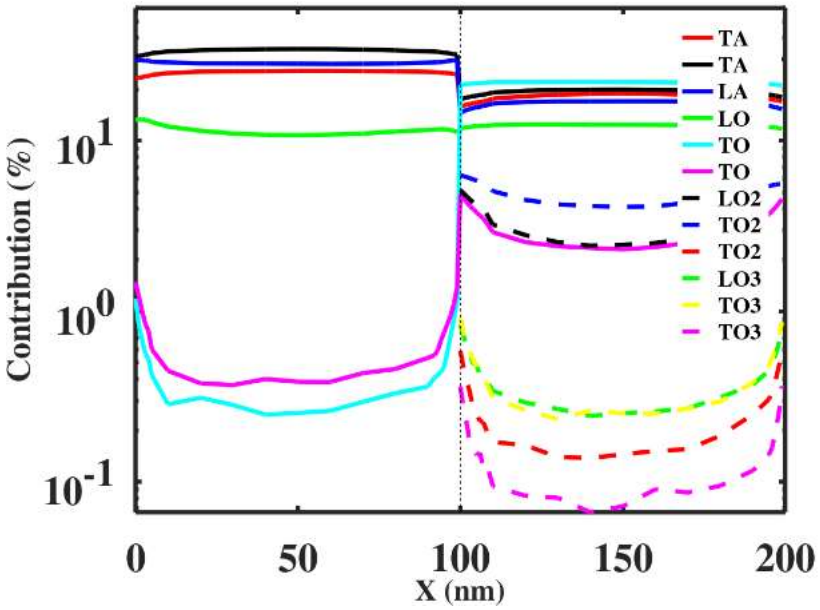

Figure 8. Modal contributions of phonons to heat transport in a 200 nm-long Polytype Ge (Cubic-Hexagonal) device

Moreover, the total of acoustic branches provides the highest contribution at all positions, which is due to their higher group velocity compared to that of optical ones. These results are very similar for polytype-Si structures (not shown).

Figure 9 generalizes these tendencies to all device lengths. In this Figure we display the modal contribution to heat transport in Polytype Ge (T_H:Ge 3C / T_C:Ge 2H) of various lengths at two different positions, i.e. $x = L/4$ (middle of Ge 3C bar, Fig. 9(a)) and $x = 3L/4$ (middle of Ge 2H bar, Fig. 9(b)).

It appears clearly that, for both 3C and 2H Ge, the contribution of acoustic to the heat flux tends to increase when increasing the device length. It is interesting to note that the optical modes cannot be ignored in the ballistic regime, i.e. in the absence of scattering in all branches, while in long devices the acoustic modes are predominant, apart from one of the TO mode in Ge 2H, the contribution of which remains significant even for the longest devices.

In longer devices in which the transport is diffusive, the modal contributions tend to be size independent. But these contributions are different in small devices of less than 100 nm when the transport is close to equilibrium. Thus, these modal flux contributions are dependent on the transport regimes and can be used as a local indicator if the contributions differ from those expected near equilibrium, i.e., in a diffusive transport regime [23].

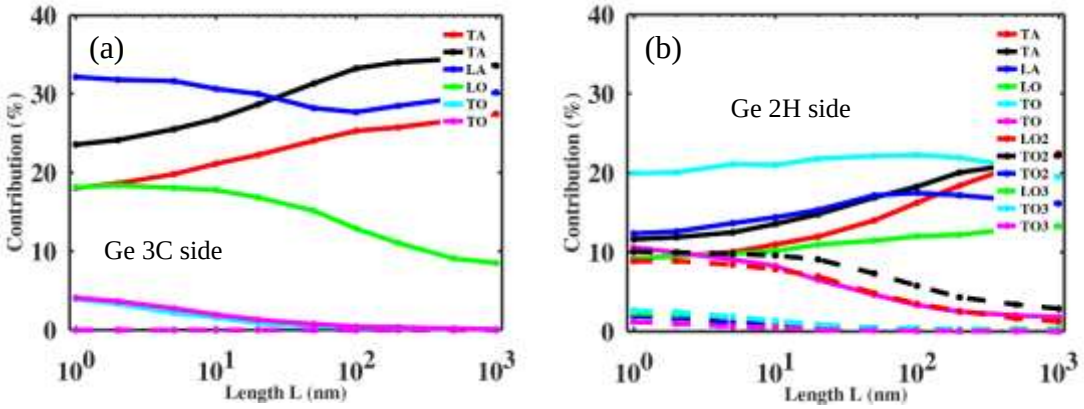

Figure 9. Modal contributions of phonons to heat transport in Polytype Ge 3C-2H devices in function of device length *L* at two different positions. (a) at *x* = L/4 (in Ge 3C) and (b) at *x* = 3L/4 (in Ge 2H).

The modal contribution profiles shown in Figure 8 are actually symmetrical when the thermostats are inverted (meaning T_H: Ge 2H / T_C: Ge 3C instead of T_H: Ge 3C / T_C: Ge 2H). The result of this configuration (not shown) is the exact mirror image of Figure 8. It is consistent with the results represented in Figure 10 that shows the modal contributions of phonons to the heat flux along a 300 nm long device containing a double heterojunction. It consists of a Ge 3C bar on the left (T_H) ($0 \leq x \leq 100$ nm), a Ge 2H bar (100 nm $\leq x \leq$ 200 nm) in the middle, and another Ge 3C bar on the right (T_C) (200 nm $\leq x \leq$300 nm). Standard thermostat temperature conditions were applied.

We witness the conservation of heat flux and stabilization of the modal contribution, going from Ge 3C to Ge 2H, or vice-versa. The DMM junctions slightly disturb the distribution of phonon modes, but they tend to re-stabilize after a few nanometres. This illustrates the appearance of a non-equilibrium transport regime around the interface.

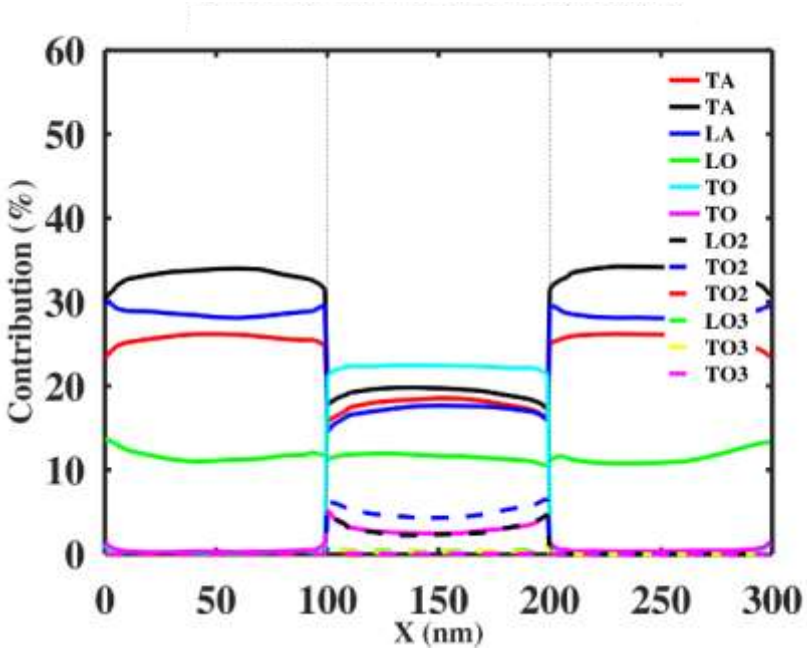

Figure 10. Modal contributions of phonons to heat transport in a 300 nm long Polytype Ge 3C-2H-3C double –heterojunction device at room temperature.

Hence, Figure 10 demonstrates the powerful capabilities of the simulator to deal with non-trivial geometries and heterostructures with multiple interfaces. It also shows that studying such a double heterostructure only needs to be done for two thirds of it, as the whole is only a mirrored result of a simpler heterostructure one.

The previous result and subsequent remarks can be extrapolated to simple and double heterostructures made of other materials, as Ge-Si or Polytype Si structures.

4. Conclusion

A Full Band Monte Carlo simulator for phonons parametrized by DFT calculation has been used to study the thermal transport in polytype Ge and Si heterojunctions.

For homogenous 3C and 2H Si and Ge bars, the thermal conductance values are almost identical in each Si and Ge type. Besides, it has been shown that the different transport regimes (diffusive, ballistic and intermediate) can be characterized by the Knudsen number as well as by the spectral contributions of the thermal flux.

In single and double polytype Si and Ge heterostructures it was shown that the polytype interfaces exhibit significant thermal resistance close the thermal conductance of the Si/Ge interface.

Finally, the modal contribution has been used as a local indicator of the occurrence the out of equilibrium transport regime. This out of equilibrium transport generated by the polytype interface occurs a few nanometers around the interface.

Acknowledgements

This work was supported by the French National Research Agency (ANR) as part of the "Investissements d'Avenir" program (Labex NanoSaclay, reference: ANR-10-LABX-0035) and the project Placho (ANR-21-CE50-0008).

Received: ((will be filled in by the editorial staff))

Revised: ((will be filled in by the editorial staff))

Published online: ((will be filled in by the editorial staff))

References

[1] "https://flowcharts.llnl.gov/content/assets/images/charts/Energy/Energy_2020_United-States.png." [Online]. Available: https://flowcharts.llnl.gov/content/assets/images/charts/Energy/Energy_2020_United-States.png

[2] J. Yan, X. Liao, D. Yan, and Y. Chen, "Review of Micro Thermoelectric Generator," *J. Microelectromech. Syst.*, vol. 27, no. 1, pp. 1–18, Feb. 2018, doi: 10.1109/JMEMS.2017.2782748. [Online]. Available: http://ieeexplore.ieee.org/document/8248771/. [Accessed: Mar. 18, 2021]

[3] L. D. Hicks and M. S. Dresselhaus, "Thermoelectric figure of merit of a one-dimensional conductor," *Physical review B*, vol. 47, no. 24, p. 16631, 1993 [Online]. Available: http://journals.aps.org/prb/abstract/10.1103/PhysRevB.47.16631. [Accessed: Oct. 19, 2015]

[4] J. P. Heremans, M. S. Dresselhaus, L. E. Bell, and D. T. Morelli, "When thermoelectrics reached the nanoscale," *Nature nanotechnology*, vol. 8, no. 7, pp. 471–473, 2013 [Online]. Available: http://www.nature.com/articles/nnano.2013.129. [Accessed: Dec. 18, 2015]

[5] V. Vargiamidis, M. Thesberg, and N. Neophytou, "Theoretical model for the Seebeck coefficient in superlattice materials with energy relaxation," *Journal of Applied Physics*, vol. 126, no. 5, p. 055105, Aug. 2019, doi: 10.1063/1.5108607. [Online]. Available: http://aip.scitation.org/doi/10.1063/1.5108607. [Accessed: May 05, 2022]

[6] R. Kim and M. S. Lundstrom, "Computational study of the Seebeck coefficient of one-dimensional composite nano-structures," *Journal of Applied Physics*, vol. 110, no. 3, p. 034511, Aug. 2011, doi: 10.1063/1.3619855. [Online]. Available: http://aip.scitation.org/doi/10.1063/1.3619855. [Accessed: Mar. 17, 2021]

[7] F. J. Lopez, U. Givan, J. G. Connell, and L. J. Lauhon, "Silicon Nanowire Polytypes: Identification by Raman Spectroscopy, Generation Mechanism, and Misfit Strain in Homostructures," *ACS Nano*, vol. 5, no. 11, pp. 8958–8966, Nov. 2011, doi: 10.1021/nn2031337. [Online]. Available: http://pubs.acs.org/doi/abs/10.1021/nn2031337. [Accessed: Jun. 16, 2017]

[8] L. Vincent *et al.*, "Novel Heterostructured Ge Nanowires Based on Polytype Transformation," *Nano Letters*, vol. 14, no. 8, pp. 4828–4836, Aug. 2014, doi: 10.1021/nl502049a. [Online]. Available: http://pubs.acs.org/doi/abs/10.1021/nl502049a. [Accessed: Feb. 16, 2016]

[9] F. X. Alvarez and D. Jou, "Size and frequency dependence of effective thermal conductivity in nanosystems," *Journal of Applied Physics*, vol. 103, no. 9, p. 094321, May 2008, doi: 10.1063/1.2913057. [Online]. Available: http://aip.scitation.org/doi/10.1063/1.2913057. [Accessed: Jan. 15, 2022]

[10] P. Kapitza, “The study of heat transfer in helium II,” *J. Phys.(USSR)*, vol. 4, no. 1–6, pp. 181–210, 1941.

[11] E. T. Swartz and R. O. Pohl, “Thermal boundary resistance,” *Reviews of modern physics*, vol. 61, no. 3, p. 605, 1989 [Online]. Available: http://journals.aps.org/rmp/abstract/10.1103/RevModPhys.61.605. [Accessed: Feb. 25, 2016]

[12] G. C. Zeng Taofang, “NONEQUILIBRIUM PHONON AND ELECTRON TRANSPORT IN HETEROSTRUCTURES AND SUPERLATTICES,” *Microscale Thermophysical Engineering*, vol. 5, no. 2, pp. 71–88, Apr. 2001, doi: 10.1080/108939501750397436. [Online]. Available: https://www.tandfonline.com/doi/full/10.1080/108939501750397436. [Accessed: Oct. 03, 2019]

[13] B. Davier, P. Dollfus, N. D. Le, S. Volz, J. Shiomi, and J. Saint-Martin, “Revisiting thermal conductivity and interface conductance at the nanoscale,” *International Journal of Heat and Mass Transfer*, vol. 183, p. 122056, Feb. 2022, doi: 10.1016/j.ijheatmasstransfer.2021.122056. [Online]. Available: https://linkinghub.elsevier.com/retrieve/pii/S0017931021011625. [Accessed: Dec. 20, 2021]

[14] N. Mingo, L. Yang, D. Li, and A. Majumdar, “Predicting the Thermal Conductivity of Si and Ge Nanowires,” *Nano Letters*, vol. 3, no. 12, pp. 1713–1716, Dec. 2003, doi: 10.1021/nl034721i. [Online]. Available: http://pubs.acs.org/doi/abs/10.1021/nl034721i. [Accessed: Jul. 01, 2015]

[15] F. Mazzamuto, J. Saint-Martin, V. H. Nguyen, C. Chassat, and P. Dollfus, “Thermoelectric performance of disordered and nanostructured graphene ribbons using Green’s function method,” *Journal of Computational Electronics*, vol. 11, no. 1, pp. 67–77, Mar. 2012, doi: 10.1007/s10825-012-0392-0. [Online]. Available: http://link.springer.com/10.1007/s10825-012-0392-0. [Accessed: Nov. 12, 2014]

[16] E. S. Landry and A. J. H. McGaughey, “Thermal boundary resistance predictions from molecular dynamics simulations and theoretical calculations,” *Physical Review B*, vol. 80, no. 16, pp. 165304–1, Oct. 2009, doi: 10.1103/PhysRevB.80.165304. [Online]. Available: https://link.aps.org/doi/10.1103/PhysRevB.80.165304. [Accessed: Sep. 11, 2017]

[17] Y. Chalopin, K. Esfarjani, A. Henry, S. Volz, and G. Chen, “Thermal interface conductance in Si/Ge superlattices by equilibrium molecular dynamics,” *Physical Review B*, vol. 85, no. 19, p. 195302, May 2012, doi: 10.1103/PhysRevB.85.195302. [Online]. Available: http://link.aps.org/doi/10.1103/PhysRevB.85.195302. [Accessed: Dec. 10, 2014]

[18] S. Merabia and K. Termentzidis, “Thermal conductance at the interface between crystals using equilibrium and nonequilibrium molecular dynamics,” *Physical Review B*, vol. 86, no. 9, Sep. 2012, doi: 10.1103/PhysRevB.86.094303. [Online]. Available: https://link.aps.org/doi/10.1103/PhysRevB.86.094303. [Accessed: Sep. 11, 2017]

[19] S. Mazumder and A. Majumdar, “Monte Carlo Study of Phonon Transport in Solid Thin Films Including Dispersion and Polarization,” *Journal of Heat Transfer*, vol. 123, no. 4, p. 749, 2001, doi: 10.1115/1.1377018. [Online]. Available: http://HeatTransfer.asmedigitalcollection.asme.org/article.aspx?articleid=1445087. [Accessed: Jul. 13, 2016]

[20] D. Lacroix, K. Joulain, and D. Lemonnier, “Monte Carlo transient phonon transport in silicon and germanium at nanoscales,” *Phys. Rev. B*, vol. 72, no. 6, p. 064305, Aug. 2005,

doi: 10.1103/PhysRevB.72.064305. [Online]. Available: https://link.aps.org/doi/10.1103/PhysRevB.72.064305

[21] J.-P. M. Peraud and N. G. Hadjiconstantinou, "Efficient simulation of multidimensional phonon transport using energy-based variance-reduced Monte Carlo formulations," *Phys. Rev. B*, vol. 84, no. 20, p. 205331, Nov. 2011, doi: 10.1103/PhysRevB.84.205331. [Online]. Available: http://link.aps.org/doi/10.1103/PhysRevB.84.205331

[22] B. Davier *et al.*, "Heat transfer in rough nanofilms and nanowires using full band *ab initio* Monte Carlo simulation," *J. Phys.: Condens. Matter*, vol. 30, no. 49, p. 495902, Dec. 2018, doi: 10.1088/1361-648X/aaea4f. [Online]. Available: http://stacks.iop.org/0953-8984/30/i=49/a=495902?key=crossref.f61afed342cd4adcd67d9a7b33713355. [Accessed: Jul. 26, 2019]

[23] N. D. Le, B. Davier, P. Dollfus, N. Izitounene, and J. Saint-Martin, "Study of phonon transport across several Si/Ge interfaces using full-band phonon Monte Carlo simulation," *Journal of Computational Electronics*, vol. to be published, May 2022 [Online]. Available: http://arxiv.org/abs/2102.10833. [Accessed: Feb. 23, 2021]

[24] L. Paulatto, I. Errea, M. Calandra, and F. Mauri, "First-principles calculations of phonon frequencies, lifetimes, and spectral functions from weak to strong anharmonicity: The example of palladium hydrides," *Phys. Rev. B*, vol. 91, no. 5, p. 054304, Feb. 2015, doi: 10.1103/PhysRevB.91.054304. [Online]. Available: https://link.aps.org/doi/10.1103/PhysRevB.91.054304. [Accessed: Apr. 21, 2021]

[25] J. Larroque, P. Dollfus, and J. Saint-Martin, "Phonon transmission at Si/Ge and polytypic Ge interfaces using full-band mismatch based models," *Journal of Applied Physics*, vol. 123, no. 2, p. 025702, Jan. 2018, doi: 10.1063/1.5007034. [Online]. Available: http://aip.scitation.org/doi/10.1063/1.5007034. [Accessed: Sep. 26, 2019]

[26] P. Reddy, K. Castelino, and A. Majumdar, "Diffuse mismatch model of thermal boundary conductance using exact phonon dispersion," *Applied Physics Letters*, vol. 87, no. 21, p. 211908, 2005, doi: 10.1063/1.2133890. [Online]. Available: http://scitation.aip.org/content/aip/journal/apl/87/21/10.1063/1.2133890. [Accessed: Dec. 03, 2015]

[27] A. Valentin, J. Sée, S. Galdin-Retailleau, and P. Dollfus, "Study of phonon modes in silicon nanocrystals using the adiabatic bond charge model," *Journal of Physics: Condensed Matter*, vol. 20, no. 14, p. 145213, Apr. 2008, doi: 10.1088/0953-8984/20/14/145213. [Online]. Available: http://stacks.iop.org/0953-8984/20/i=14/a=145213?key=crossref.56c2a189b3e2acab0b2fc962236fb21e. [Accessed: Feb. 16, 2016]

[28] P. Giannozzi *et al.*, "Quantum ESPRESSO: a modular and open-source software project for quantum simulations of materials," *J. Phys.: Condens. Matter*, vol. 21, no. 39, p. 395502, Sep. 2009, doi: 10.1088/0953-8984/21/39/395502. [Online]. Available: http://arxiv.org/abs/0906.2569. [Accessed: Sep. 26, 2019]

[29] J. P. Perdew and A. Zunger, "Self-interaction correction to density-functional approximations for many-electron systems," *Phys. Rev. B*, vol. 23, no. 10, pp. 5048–5079, May 1981, doi: 10.1103/PhysRevB.23.5048. [Online]. Available: https://link.aps.org/doi/10.1103/PhysRevB.23.5048. [Accessed: Jan. 24, 2022]

[30] M. Schlipf and F. Gygi, "Optimization algorithm for the generation of ONCV pseudopotentials," *Computer Physics Communications*, vol. 196, pp. 36–44, Nov. 2015,

doi: 10.1016/j.cpc.2015.05.011. [Online]. Available: https://linkinghub.elsevier.com/retrieve/pii/S0010465515001897. [Accessed: Jan. 24, 2022]

[31] P. Giannozzi *et al.*, "Advanced capabilities for materials modelling with Quantum ESPRESSO," *J. Phys.: Condens. Matter*, vol. 29, no. 46, p. 465901, Nov. 2017, doi: 10.1088/1361-648X/aa8f79. [Online]. Available: https://iopscience.iop.org/article/10.1088/1361-648X/aa8f79. [Accessed: Jan. 24, 2022]

[32] L. Paulatto, F. Mauri, and M. Lazzeri, "Anharmonic properties from a generalized third-order *ab initio* approach: Theory and applications to graphite and graphene," *Phys. Rev. B*, vol. 87, no. 21, p. 214303, Jun. 2013, doi: 10.1103/PhysRevB.87.214303. [Online]. Available: https://link.aps.org/doi/10.1103/PhysRevB.87.214303. [Accessed: Apr. 21, 2021]

[33] J.-P. M. Péraud, C. D. Landon, and N. G. Hadjiconstantinou, "Monte carlo methods for solving the boltzmann transport equation," *Annual Review of Heat Transfer*, vol. 17, pp. 205–265, 2014, doi: http://dx.doi.org/10.1615/AnnualRevHeatTransfer.2014007381. [Online]. Available: http://www.dl.begellhouse.com/pt/download/article/1d883b612ccfafde/ARHT(7)-7381.pdf. [Accessed: Nov. 02, 2015]

[34] B. Davier *et al.*, "Heat transfer in rough nanofilms and nanowires using full band *ab initio* Monte Carlo simulation," *Journal of Physics: Condensed Matter*, vol. 30, no. 49, p. 495902, Dec. 2018, doi: 10.1088/1361-648X/aaea4f.

[35] C. J. Glassbrenner and G. A. Slack, "Thermal conductivity of silicon and germanium from 3 K to the melting point," *Physical Review*, vol. 134, no. 4A, p. A1058, 1964 [Online]. Available: https://journals.aps.org/pr/abstract/10.1103/PhysRev.134.A1058. [Accessed: Sep. 03, 2017]